RSC Advances

PAPER

View Article Online
View Journal | View Issue

Cite this: *RSC Adv.*, 2017, **7**, 38861

A novel synthesis protocol for Co_3O_4 nanocatalysts and their catalytic applications†

M. Sivachidambaram,[a] J. Judith Vijaya,*[a] K. Kaviyarasu,[bc] L. John Kennedy,[d] Hamad A. Al-Lohedan[e] and R. Jothi Ramalingam[e]

Co_3O_4 spinel nanoparticles (Co_3O_4-NPs) are synthesized *via* a green route using neem (*Azadirachta indica*) leaf by an efficient and simple hot plate combustion method (HPCM). The as-prepared Co_3O_4-NPs have been characterized by well-known recognized techniques such as X-ray diffraction (XRD), high resolution transmission electron microscopy (HRTEM), energy dispersive X-ray analysis (EDX), diffuse reflectance spectroscopy (DRS), photoluminescence spectroscopy (PL), Raman spectroscopy, and vibrating sample magnetometry (VSM). Co_3O_4-NPs were investigated in various application areas; for example, a multi-lamp photocatalytic reactor was used to degrade the hazardous textile dye waste (TDW) collected from the dyeing industry. Furthermore, the antimicrobial activity of the synthesized Co_3O_4-NPs was studied against Gram-positive (*Staphylococcus aureus* and *Bacillus subtilis*) and Gram-negative (*Pseudomonas aeruginosa* and *Escherichia coli*) bacteria, in comparison to a chloramphenicol standard, and also evaluated by carrying out the catalytic hydrogenation of 4-nitrophenol and 4-nitroaniline in the presence of $NaBH_4$ as a reducing agent. Noble metals have been reported earlier, but due to their high cost they needed to be replaced by a cost effective material. We have also discussed feasible mechanisms and catalytic activity of the Co_3O_4-NPs in different applications. Thus, we have proposed a novel, economic and green synthesis of Co_3O_4-NPs that is highly important in the present times for the removal of hazardous chemicals.

Received 23rd June 2017
Accepted 22nd July 2017

DOI: 10.1039/c7ra06996k

rsc.li/rsc-advances

Introduction

The use of green synthesis methods for the preparation of metal nanoparticles provides advancement over various methods as they are simple, one step, cost-effective, environment friendly, relatively reproducible and often result in more stable materials.[1] Physical and chemical methods can also be utilized to produce nanoparticles, but the rates of synthesis are slow compared to those of the routes involving plant-mediated syntheses.[2] Although, the potential of higher plants as sources for this purpose is still largely unexplored, very recently, plant extracts of marigold flower,[3] *Ziziphora tenuior*,[4] *Abutilon indicum*,[5] *Solanum trilobatum*,[6] *Erythrina indica*[7] and *Sesuvium portulacastrum*[8] were reported in the literature as a source for the synthesis of metal nanoparticles with sizes ranging from 5 to 20 nm, as an alternative to the physical and chemical methods.

Numerous investigations have been carried out on the chemistry of *Azadirachta indica* (*A. indica*) tree products. All parts of the *A. indica* tree, such as the leaves, flowers, seeds, roots and bark, have been used in traditional medicine as household remedies against various human ailments. Various medicinal utilities have been described, particularly for *A. indica* leaf.[9] *A. indica* leaves exhibit a wide range of pharmacological activities and medicinal applications and have been used extensively as ingredients in ancient medicinal preparations because of their availability throughout the year as well as the ease of extracting the compounds.[10] *A. indica* leaves contain 0.13% essential oil, which is responsible for the smell of the leaves.[11] In particular, the leaf of *A. indica* is a 'storehouse' of more than 140 active organic compounds that are chemically diverse and structurally complex. These compounds are divided into two major classes: isoprenoids and non-isoprenoids. The isoprenoids include diterpenoids, triterpenoids, vilasinin type of compounds, limonoids and their derivatives, and C-secomeliacins. The non-isoprenoids include proteins, polysaccharides, sulphur compounds, flavonoids, dihydrochalone,

[a]*Catalysis & Nanomaterials Research Laboratory, Department of Chemistry, Loyola College (Autonomous), Chennai 600 034, India. E-mail: jjvijaya78@gmail.com; Fax: +91-44-28175566; Tel: +91-44-28178200*

[b]*UNESCO-UNISA Africa Chair in Nanosciences/Nanotechnology Laboratories, College of Graduate Studies, University of South Africa (UNISA), Muckleneuk Ridge, P O Box 392, Pretoria, South Africa*

[c]*Nanosciences African Network (NANOAFNET), Materials Research Group (MRG), iThemba LABS-National Research Foundation (NRF), 1 Old Faure Road, 7129, P O Box 722, Somerset West, Western Cape Province, South Africa*

[d]*Materials Division, School of Advanced Sciences, Vellore Institute of Technology (VIT) University, Chennai Campus, Chennai 600 127, India*

[e]*Surfactant Research Chair, Chemistry Department, College of Science, King Saud University, Riyadh 11451, Saudi Arabia*

† Electronic supplementary information (ESI) available. See DOI: 10.1039/c7ra06996k

coumarin, tannins and aliphatic compounds.[12] Considering the massive potentiality of *A. indica* leaves, they can be used as a source in a biological green technique for the synthesis of cobalt oxide nanoparticles. In this regard, leaf extract of *A. indica* (commonly known as neem), a species of the Meliaceae family, was used as a capping and stabilizing agent to synthesize cobalt oxide NPs by a hot plate combustion method (HPCM). Cobalt oxide NPs can be produced using a low concentration of *A. indica* leaf extract without using any additional harmful chemical/physical reagents.

Cobalt oxide is a transition metal oxide and it occurs in five different oxidation states, such as Co, CoO_2, Co_2O_3, CoO(OH), CoO and Co_3O_4.[13,17] Furthermore, Co_3O_4 exhibits mixed oxidation states like Co^{2+} and Co^{3+}, and it has a regular cubic spinel structure with the tetrahedral sites (8a) occupied by Co^{2+} ions and the octahedral sites (16d) by Co^{3+} ions.[14] It is a p-type semiconductor, anti-ferromagnetic, highly stable and easy to synthesize in open air atmosphere. Co_3O_4-NPs can be synthesized by various methods, such as, electrodeposition,[15] and hydrothermal,[16] solvothermal,[17] polyol,[18] and thermal decomposition.[19] Because of their unusual physical, chemical, magnetic and electronic properties, they have vast applications for use in electrochromic devices, gas sensors, supercapacitors, solar selective absorbers, fuel cells, catalytic applications and lithium ion batteries.[20] Due to their low cost in comparison to the high cost noble metal NPs, they work as effective catalysts in heterogeneous chemical reactions.[21] Some expensive noble metals have also been reported for applications in photocatalytic degradation such as the photo-electro-catalytic oxidation of the antibiotic tetracycline[22] (73% removal efficiency using Au nanoclusters/TiO_2 nanotube array); moreover, noble metals have been known to exhibit antimicrobial activity against Gram-positive bacteria like *S. epidermidis*, *B. subtilis*, and Gram-negative bacteria like *E. coli* and *P. aeruginosa*, where 90% of the bacterial population was killed by Au nanoclusters (NCs).[23] AgNCs-daptomycin hybrid (D-AgNCs) provided the highest killing effect against the Gram-positive model bacterium *Staphylococcus aureus* (*S. aureus*).[24] These revelations raised an interest in us to employ Co_3O_4-NPs in three different applications. Hence, in the present study, we synthesized Co_3O_4-NPs using *A. indica* leaf extract by an efficient green HPCM method, and the catalytic activity towards the photodegradation of textile dye waste (TDW) and the catalytic hydrogenation of 4-nitroaromatics (4-nitrophenol and 4-nitroaniline) was determined. The antibacterial activity against Gram-positive (*Staphylococcus aureus* and *Bacillus subtilis*) and Gram-negative (*Pseudomonas aeruginosa* and *Escherichia coli*) bacteria is also reported.

Experimental section

Materials and methods

Cobalt(II) nitrate hexahydrate, $Co(NO_3)_2 \cdot 6H_2O$ (Sigma-Aldrich, purity ≥ 98%), and glycine, $C_2H_5NO_2$ (Sigma-Aldrich, purity ≥ 98.5%), are the primary requirements for the synthesis of Co_3O_4-NPs. Sodium borohydride, $NaBH_4$ (≥98.0%), 4-nitrophenol (≥99.0%) and 4-nitroaniline (≥99.0%) from Sigma-Aldrich were used for the catalytic reduction. For the examination of antibacterial potential, two microbiological media, Muller Hinton Agar (MHA) and Nutrient Broth (NB), and the commercial antibiotic, chloramphenicol, were purchased from Hi-Media Laboratories (Mumbai, India). De-ionized H_2O obtained after sanitization through a Millipore system was used throughout the experiments. The rest of the chemicals was used without further purification.

Synthesis of Co_3O_4-NPs

An aqueous solution of cobalt(II) nitrate ($Co(NO_3)_2 \cdot 6H_2O$), *Azadirachta indica* (*A. indica*) leaf extract (5 mL) and glycine ($C_2H_5NO_2$) was used to synthesize the Co_3O_4-NPs *via* HPCM. The stoichiometric ratio of the precursors was used to synthesize the Co_3O_4-NPs and, finally 1.8 g of Co_3O_4-NPs was obtained. Primarily, the precursors were dissolved in 70 mL of deionized water and kept aside for 1 h with constant stirring to attain a homogenous solution. In the HPCM, the above homogeneous solution was placed in a hot plate (Barnstead Thermolyne, model no: SP46925) and uniformly heated up to 250 °C for 15 min, which led to the volatilization of water and combustion of the reaction mixture. The black coloured precipitate was then separated by centrifugation and washed several times with deionized water. The separated black powder was dried at 100 °C in a hot air oven and subjected to annealing at 300 °C for 2 h.

Analytical methods for catalyst characterization

X-ray diffraction (XRD) patterns were studied on a Siemens D5000 diffractometer using Cu Kα radiation in the continuous scan mode to collect data over the 2θ range of 10–90°. The Raman active modes of vibration were observed on the Raman spectrophotometer (STR-250 Seki Technotron Corporation). A high-resolution transmission electron microscopy (HRTEM) analysis was carried out, wherein a Jeol JEM 4000EX electron microscopy unit with a resolution limit of about 0.12 nm equipped with a Gatan digital camera was employed for imaging and size and shape analysis of Co_3O_4-NPs. The chemical composition of the synthesized sample was confirmed by Energy Dispersive X-ray Spectroscopy (EDX) using an Oxford instruments X Max solid-state Silicon drift detector operating at 20 keV. Magnetization measurements of the samples were performed on a Quantum Design Model 6000 vibrating sample magnetometer (VSM). The diffuse reflectance UV-visible spectra of Co_3O_4-NPs were recorded on Cary100 UV-visible spectrophotometer to estimate the energy band gaps. In addition, the emission spectra were recorded using a Varian Cary Eclipse Fluorescence Spectrophotometer at an excitation wavelength of 370 nm.

Photocatalytic degradation procedure and setup

A multi-lamp photocatalytic reactor was used to degrade the hazardous textile dye waste (TDW) collected from the dyeing industry at Tuticorin, Tamil Nadu, India. The reactor was fitted with low pressure mercury lamps (8/8 W), which could emit UV radiation. From our trial experiments, we confirmed that the

wavelength of 365 nm is more suitable for the PCD of hazardous TDW. The borosilicate reactor tubes were designed in such a way that they could hold 100 mL of the hazardous TDW dye solution. The experimental procedure for performing the PCD reaction is as follows. The initial COD of the hazardous TDW was fixed (in mg L^{-1}), a known amount of Co_3O_4-NPs was added to this solution and placed in the dark for 12 h to attain adsorption equilibrium, and the resultant COD was estimated. The above mentioned solution was placed inside the photocatalytic reactor and irradiated with UV light for 2.30 h. Equal aliquots were taken from the reactor tube at regular intervals of 30 min, followed by centrifugation and continuous recording of the UV spectra of the collected samples. The percentage of COD removal was calculated *via* the eqn (1):

$$\%\ \text{removal of COD (mg L}^{-1}) = (\text{initial COD} - \text{final COD/initial COD}) \times 100 \quad (1)$$

According to the recommendation of the Indian pollution control board standard, the hazardous TDW discharged from the textile dyeing industries into the aqua ecosystem must not exceed 250 mg L^{-1} COD,[25] and therefore the PCD of hazardous TDW was analyzed using Co_3O_4-NPs to reduce the levels below 250 mg L^{-1} COD.

Catalytic reduction of 4-nitrophenol and 4-nitroaniline

The reactant 4-nitrophenol (1.7 mL) was added to an ice cold aqueous solution of sodium borohydride (1 mL) taken in a standard quartz cuvette. The light yellow colour of 4-nitrophenol was gradually transformed to yellowish green due to the 4-nitrophenolate ion formation. Then, a known amount of Co_3O_4-NPs (0.02 g) synthesized by HPCM was added to the above solution, and the time-dependent UV-visible absorbance spectra of the resultant solution were incessantly monitored at regular intervals of 30 s. Catalytic reduction of 4-nitroaniline was also followed by the same experimental procedure.

Analysis of the antibacterial potential of Co_3O_4-NPs

The antibacterial potential of the Co_3O_4-NPs was investigated against Gram-positive and Gram-negative bacterial strains by the disk diffusion method. In total, four bacterial strains, which included two Gram-positive bacteria (*Staphylococcus aureus*, *Bacillus subtilis*) and two Gram-negative bacteria (*Pseudomonas aeruginosa*, *Escherichia coli*) were chosen for the investigation. The bacteria were sub-cultured from pure cultures of different strains of bacteria on nutrient broth overnight at 37 °C. The turbidity of the bacterial cultures was maintained at 0.5 McFarland standard equivalence. Each bacterial strain was swabbed uniformly onto the surface of Mueller–Hinton agar medium in isolated agar plates using sterile cotton swabs under sterile conditions. The sterile paper disks were placed on the agar plates and 10 μL of 0.001 g/10 μL (w/v) of Co_3O_4-NPs was added into the disks. The antibiotic chloramphenicol (10 mcg per disk) was chosen as the standard drug for the determination of the antibacterial potential of Co_3O_4-NPs. All the strains of bacteria treated with Co_3O_4-NPs and chloramphenicol were incubated at 37 °C for 24 h. The antibacterial tests were performed in duplicates. The zones of inhibition were measured, which appeared as a clear area in each disk, and then compared with the standard chloramphenicol.

Results and discussion

The Co_3O_4-NPs prepared in the present study have several advantages including being environmentally friendly, their synthesis possessing economy in time of preparation, and incorporating commonly available and cost-effective chemicals such as cobalt(II) nitrate and glycine. In order to compare the various chemicals used for the synthesis of Co_3O_4-NPs with those used in other reported methods, Table 1 is presented.

X-ray diffraction studies were used to resolve the structural properties of the Co_3O_4 prepared using HPCM. The X-ray diffraction patterns show eight peaks at 31.27°, 36.86°, 38.57°, 44.82°, 55.69°, 59.38°, 65.26°, and 79.12°, which correspond to the (220), (311), (222), (400), (422), (511), (440), and (620) planes that are in the cubic phase of Co_3O_4,[29] respectively, (JCPDS card no. 43-1003). The size of the Co_3O_4 nanoparticles was calculated from the (311) diffraction peak using the Debye–Scherrer eqn (2):

$$L = \frac{K\lambda}{\beta \cos\theta} \quad (2)$$

Table 1 Co_3O_4-NPs synthesized by different methods using different chemicals

S/no	Reference	Chemicals used	Method
1	L. M. Alrehaily *et al.*, 2015 (26)	N_2O gas, argon, nano pure diamond UV ultrapure water system, gamma source, cobalt chloride and *t*-butanol	Radiation-induced formation
2	Rodolfo Foster Klein Gunnewiek *et al.*, 2016 (27)	Ammonium polyacrylate and cobalt nitrate	Modified-polymeric precursor method
3	Clément J. Denis *et al.*, 2015 (28)	CHFS process, cobalt(II) acetate, ethanol and nano pure diamond UV ultrapure water system	Hydrothermal reactor under laminar and turbulent flow
4	Present work	Cobalt(II) nitrate hexahydrate, glycine and *Azadirachta indica*	Hot plate combustion method

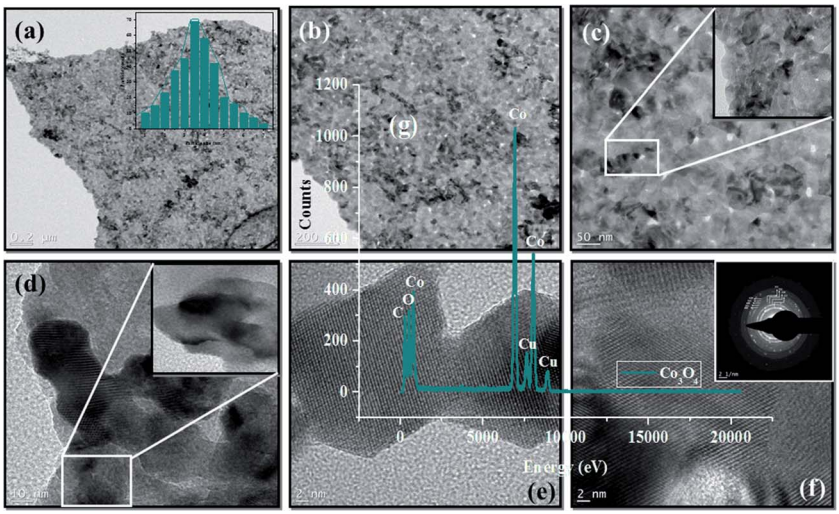

Fig. 1 (a–f) HR-TEM, inset (a and f) particle size distribution of histogram and SAED pattern, and (g) energy dispersive X-ray (EDX) analysis of Co_3O_4-NPs.

where L is the mean dimension of the particle, θ is the diffraction angle, λ is the wavelength of the used Cu-Kα radiation, β is the full width of at half maximum (FWHM) of the diffraction peak and k is the diffraction constant (0.89). The calculated average size was about 0.24 nm, which is in good agreement with the HR-TEM results (X-ray diffraction pattern of Co_3O_4-NPs is given in the ESI, Fig. S1†).

Raman spectroscopy studies were carried out at room temperature and were used to support the immaculateness of the synthesized Co_3O_4 nanoparticles. As previously highlighted, Co_3O_4 has Co^{2+} ($3d^7$) and Co^{3+} ($3d^6$) located at tetrahedral and octahedral sites, respectively. For a spinel, the space group theory of crystallites predicts the following active modes as "*Fd*3*m*" symmetry as represented in eqn (3):

$$\Gamma = A_{1g}(R) + E_g(R) + F_{1g}(IN) + 3F_{2g}(R) + 2A_{2u}(IN) + 2E_u(IN) + 4F_{1u}(IR) + 2F_{2u}(IN), \quad (3)$$

where (R), (IR), and (IN) symbolize Raman active vibrations, infrared-active vibrations, and inactive modes, respectively. One can discriminate six active Raman modes; they are in the region of ~145, ~465.2, ~506.4, ~603, ~676.8, and ~755.5 cm^{-1}. Apart from the last mode, all the observed modes are in concurrence with the values of pure Co_3O_4 spinel structure, with an average shift of the order of $\Delta\nu \sim 5$ cm^{-1} (191, 470, 510, 608, and 675 cm^{-1}). Although, the Raman mode at 684.5 cm^{-1} is ascribed to the uniqueness of the octahedral A_{1g} sites, the E_g, and F_{2g} modes are related to the combined vibrations of the tetrahedral site and octahedral oxygen motions.[29] The average shift of $\Delta\nu \sim 5$ cm^{-1} is accredited to the size effects or surface stress/strain (Raman spectra of Co_3O_4-NPs is given as ESI, Fig. S2†).

High resolution transmission electron microscopy (HRTEM) analysis was used to examine the morphology of Co_3O_4-NPs at different magnification ranges. Co_3O_4-NPs possess high agglomeration with nearly quasi-spherical like shapes as shown in Fig. 1(a–g). During the sample processing in the HRTEM analysis, the high degree of agglomeration is due to the association of Co_3O_4-NPs in the highly concentrated sample.[30] The Co_3O_4-NPs ranged in sizes of 1–7 nm, with most of the particles being about 3.5 nm in size, as shown in the inset histogram of Fig. 1a. Co_3O_4-NPs showed a polycrystalline nature, which was confirmed by selective area electron diffraction (SAED) analysis, as shown in the inset of Fig. 1f. This pattern was obtained due to the successive reflections correlated to (111), (220), (311), (222), (400), (422), (511), (440), and (620) lattice planes, which is well in agreement with our XRD results. The fringe spacing corresponding to the (311) lattice plane was measured to be 0.24 nm, which is in good agreement with the values reported in other experimental studies.[31] The lattice planes of (111), (220), (311), (222), (400), (422), (511), (440), and (620) are correlated, due to the successive reflections of the observed SAED patterns, which are in good agreement with our XRD results. The lattice plane (311) was measured to be 0.21 nm and it corresponds to fringe spacing, which is in good agreement with the literature.[32] The maximum purity of the Co_3O_4-NPs produced was confirmed by energy dispersive X-ray analysis (EDX), which showed the clear visible peaks of the respective cobalt and oxygen atoms. During the course of sampling, the sample was placed in a carbon coated copper grid sample holder and it clearly showed the noticeable peaks of copper and carbon presence in the EDX spectrum.

Co_3O_4-NPs exhibits photoluminescence (PL) at room temperature (PL spectra are given in the ESI, Fig. S3†). The surface morphology and the structures of Co_3O_4-NPs are closely dependent on their optical properties. Usually, the PL emission of metal oxide nanostructures is classified into two sections, including near band edge (NBE) UV emission and deep level (DL) defect associated with the visible emission. The radiative recombination of a photo-generated hole is a reason for the origin of visible emission and it is caused by the impurities and structural defects in the crystal, for instance, oxygen vacancies

and cobalt interstitials. The direct recombination of the excitons through an exciton–exciton scattering is commonly attributed to the occurrence of UV emission. The absorption bands at $\lambda \sim 415$ and 500 nm were assigned to the intervalence charge-transfer $Co^{2+} \leftrightarrow Co^{3+}$, which represent the internal oxidation–reduction process and also the absorption peaks present at $\lambda \sim 500$ nm, and indicate the ligand–metal charge transfer events $O^{2-} \rightarrow Co^{3+}$ and $O^{2-} \rightarrow Co^{2+}$, respectively.[33] The set of peaks observed at $\lambda \sim 492$ and 520 nm may be due to green emission. From the spectrum, it is noted that the intensity of the UV emission is more dominant than the visible emission intensity, which reveals that the surface morphology plays an important role in the determination of optical properties. It is evident that the strong UV emission between the shallow donors (related to oxygen vacancies) from the irradiative transitions and suppressed visible emission confirmed the good crystalline nature of the Co_3O_4-NPs, as previously reported.[34]

UV-visible diffuse reflectance spectroscopy (DRS) was used to investigate the optical properties of the Co_3O_4-NPs at room temperature. The Co_3O_4-NPs possess direct transitions from the visible spectral region, because the nanoparticles behave as a semiconductor material.[35] The optical band gap (E_g) can be calculated using the Kubelka–Munk (K–M) model,[36] and the $F(R)$ value is estimated from the following eqn (4),

$$F(R) = (1 - R)^2/2R \quad (4)$$

where $F(R)$ is the Kubelka–Munk function, and R is the reflectance. The band gap can be estimated by extrapolating the linear region of the plot of $[F(R)h\nu]^2$ *versus* the photon energy, and it was found that two optical band gaps (E_g) were formed for the Co_3O_4-NPs sample. The bandgap of 1.89 eV can be associated with the $O^{2-} \rightarrow Co^{2+}$ charge transfer process (valence to conduction band excitation), while the 2.52 eV bandgap relates to the $O^{2-} \rightarrow Co^{3+}$ charge transfer (with the Co^{III} level located below the conduction band).[36] As shown in the literature,[37] the E_g values of Co_3O_4-NPs are greater than those of bulk Co_3O_4-NPs (E_g = 1.77 and 3.17 eV, respectively). The specific assigned values of the two band gaps prove that the samples are pure and belong to the p-type semiconductor.[37] The band gap energy of the Co_3O_4-NPs increases, which is an indication of the quantum confinement effect arising from the tiny crystallites.[38] (DRS spectra of Co_3O_4-NPs are attached as ESI, Fig. S4†).

The magnetic hysteresis measurements of Co_3O_4-NPs were recorded at room temperature. At the time of applied magnetic field, the magnetization (M–H) curve showed apparent linear behavior with no coercivity and remanence. Even at a high applied magnetic field of 4 kOe, no saturation occurred. This is definitely due to the anti-ferromagnetic barter interaction between the tetrahedral A sites and octahedral B sites occupied by cobalt ions in the spinel structure of Co_3O_4, resulting in zero net magnetization as a significance of complete magnetic spin reparation in magnetic sublattices.[39] It is also evident that there is no manifestation of super paramagnetism over and above and no occurrence of magnetic impurities in Co_3O_4-NPs (magnetization *vs.* magnetic field loop of Co_3O_4-NPs is given as ESI, Fig. S5†).

Co_3O_4-NPs were used in a pilot reaction for the PCD experiments in order to demonstrate their photocatalytic ability. Under UV light irradiation, the COD removal efficiency was evaluated for the hazardous textile dye waste (TDW). The disappearance of color affirms the degradation of the organic compounds in hazardous TDW when the COD level is decreased. UV-visible spectrophotometry was used to examine the photocatalytic activity of Co_3O_4-NPs on the degradation of hazardous TDW with continuous monitoring of the absorbance intensity of hazardous TDW; the COD removal efficiency was found to be affected by two tentative operating parameters, *i.e.*, catalyst loading and the pH of the medium. The initial concentration was fixed at 650 mg L^{-1} and the degradation of hazardous TDW was investigated using different amounts of Co_3O_4-NPs loading. Evidently, the results show a linear increase in the COD removal efficiency with an increase in the catalyst dosage up to the optimum level of 40 mg of catalyst. Furthermore, the COD removal efficiency decreases when the catalyst dosage is increased, which is due to the formation of active sites on the catalyst surface, which increases to produce more hydroxyl radicals ($^{\bullet}OH$) and superoxide radicals ($^{\bullet}O_2^-$).[40] However, the formation of the NP agglomeration is due to further increments in the catalyst dosage and it can block the UV light illumination on the surface of the Co_3O_4 photocatalyst, which can hold back the production of ($^{\bullet}OH$) radical, which is a primary oxidant in COD experiments.[40] The positive holes (h^+) are accountable for the major oxidation species on the surface of the Co_3O_4 photocatalyst, the produced H^+ ions are adsorbed, thus resulting in the catalyst surface being positively charged. These adsorbed positively charged Co_3O_4-NPs support the excitation of photo-induced electrons, which would react with the adsorbed O_2 molecules to produce superoxide radical anion ($^{\bullet}O_2^-$).[41] Moreover, positively charged Co_3O_4-NPs would also restrict the recombination of excited electrons and positive holes and produce more hydroxyl radicals ($^{\bullet}OH$) by the reaction between the positive holes and water molecules. Both the

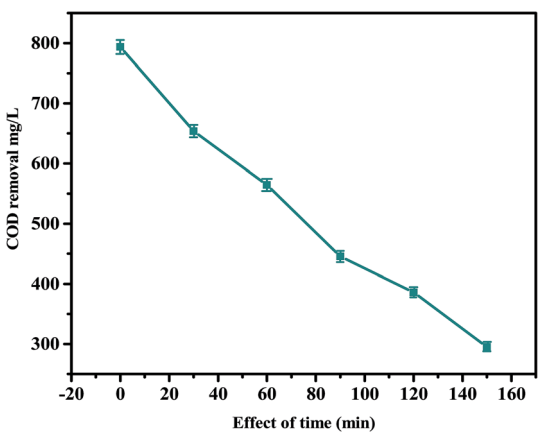

Fig. 2 Effect of time on the PCD of TDW in the presence of Co_3O_4-NPs (experimental conditions: initial concentration of TDW = 650 mg L^{-1} of COD, catalyst loading = 50 mg, λ = 365 nm).

radicals $^{\bullet}O_2^-$ and $^{\bullet}OH$ are proven to be strong oxidants and are responsible for the enhanced photodegradation of hazardous TDW.

The kinetic studies of the PCD of hazardous TDW using Co_3O_4-NPs were also performed by employing the optimized parameters of $t = 150$ min, initial concentration = 750 mg L^{-1} COD, photocatalyst dosage = 40 mg, light intensity = 365 nm and pH = 2. Fig. 2 shows the extent of COD removal (mg L^{-1}) with respect to time (min) in the presence of Co_3O_4-NPs during the PCD reaction and the COD removal efficiency of Co_3O_4-NPs in the degradation of hazardous TDW was calculated to be 73.86% after 150 min. The PCD reaction was stopped at 150 min because at this specific time, the concentration level of COD in hazardous TDW was found to be below 250 mg L^{-1} (as per the standards of the Indian pollution control board for industrial waste water let-out into river bodies). This reaction can be expressed using pseudo-first order kinetics by the following the eqn (5)

$$\ln(C_t/C_0) = -k_1 t \quad (5)$$

where k is the pseudo first order rate constant (min^{-1}), C_0, the initial concentration of hazardous TDW (750 mg L^{-1}) and C_t, the concentration of hazardous TDW at reaction time t (min). A pseudo first-order rate constant value of 1.03×10^{-3} min^{-1} was obtained from the slope of the linear plot of $\ln(C_t/C_0)$ *versus* irradiation time (the corresponding plot is given as ESI; Fig. S6.†) The possible degradation mechanism is shown in Scheme 1.

$$Co_3O_4 + h\nu \rightarrow h^+ + e^- \quad (6)$$

$$H_2O + h^+ \rightarrow H^+ + OH^{\bullet} \quad (7)$$

$$O_2 + e^- \rightarrow {}^{\bullet}O^{2-} \quad (8)$$

$$TDW + (OH^{\bullet}/{}^{\bullet}O^{2-}) \rightarrow \text{degradation products} \quad (9)$$

$$TDW + h\nu \rightarrow TDW^* \quad (10)$$

$$TDW^* + Co_3O_4 \rightarrow TDW^+ + Co_3O_4(e) \quad (11)$$

$$Co_3O_4(e) + O_2 \rightarrow {}^{\bullet}O^{2-} + Co_3O_4 \quad (12)$$

In above mechanism, the first three steps [(6)–(8)] involves the formation of active species for the PCD reaction, such as $^{\bullet}O_2^-$ and $^{\bullet}OH$ radicals obtained due to the illumination of UV light on the surface of Co_3O_4-NPs and the TDW degradation takes place in step (9). The steps (10)–(12) account for the sensitization of TDW molecules under the illumination of UV light and this process is able to insert the electrons into the crystal lattice of Co_3O_4-NPs, which would ultimately lead to the formation of $^{\bullet}O_2^-$ ions upon reaction with O_2 molecules, and would be utilized in the PCD reaction.

The catalytic activity of Co_3O_4-NPs was tested in the hydrogenation reaction using 4-nitrophenol and 4-nitroaniline, which is the most often used catalytic hydrogenation reaction. Hence, we selected two chemical reactions as model reactions *i.e.* the reduction of 4-nitrophenol and 4-nitroaniline by using

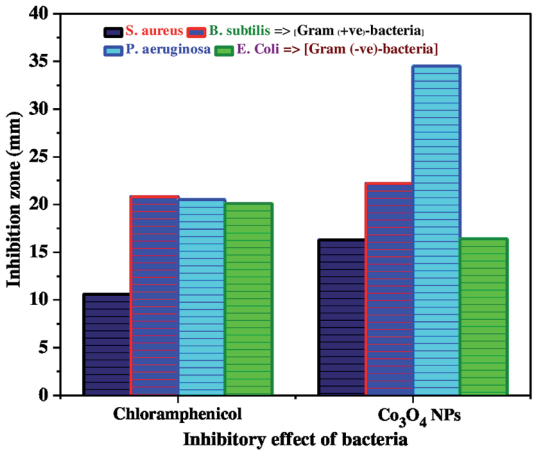

Fig. 3 Time course profile for the catalytic reduction of (a) 4-nitrophenol, and (b) 4-nitroaniline using Co_3O_4-NPs.

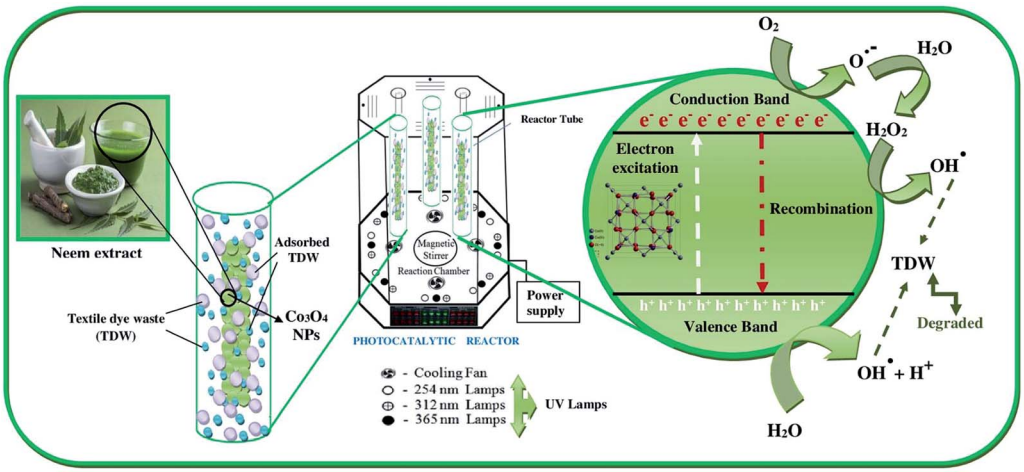

Scheme 1 PCD mechanism of TDW using Co_3O_4-NPs.

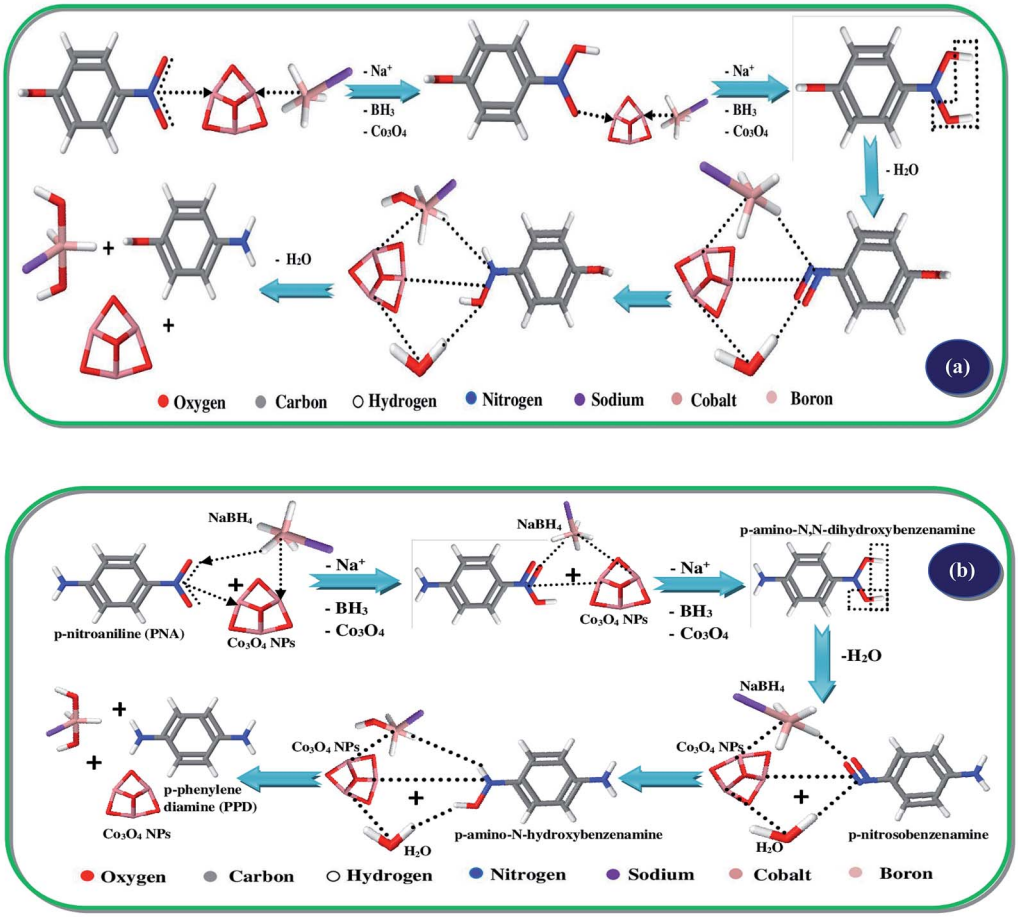

Scheme 2 Catalytic hydrogenation mechanism of (a) 4-nitrophenol, and (b) 4-nitroaniline using Co_3O_4-NPs.

the reducing agent, sodium borohydride ($NaBH_4$).[42,43] This reaction was continuously monitored at small timing intervals using UV-visible spectroscopy (Fig. 3). The strong absorption of 4-nitro-*N*,*N*-dihydroxybenzenamine at 400 nm was initially pragmatic, however a time profile study showed a significant decrease in absorption within 180 s. This appears to be a well-

Table 2 Comparison of Co_3O_4-NPs prepared by different methods and their catalytic activity

S/no	Literature	Synthesis methods	Application	Catalytic activity
1	Ravi Dhas *et al.* 2015 (44)	Surfactant method is used to prepare Co_3O_4 NPs	Photocatalytic degradation of rhodamine B	78% degradation achieved in 180 min
2	Saeed Farhadi, *et al.* 2016 (45)	Thermal decomposition of cobalt oxide complex to synthesize Co_3O_4 NPs	Photocatalytic degradation of methylene blue	74% degradation achieved in 150 min
3	Ismat Bibi, *et al.* 2017 (46)	Green and eco-friendly synthesis of cobalt-oxide nanoparticle by *Punica granatum* peel extract	Photocatalytic degradation of Remazol Brilliant Orange 3R (RBO 3R) dye	78.5% degradation achieved in 180 min
4	Sharma, *et al.* 2017 (47)	Co doped CuO by precipitation method	Reduction of 4-nitrophenol to 4-aminophenol	Reduction occurred at λ_{max} = 403 nm in 180 s
5	Jan Krajczewski, *et al.* 2016 (48)	Pt doped cobalt oxide NPs	Reduction of 4-nitrophenol to 4-aminophenol	Reduction occurred at λ_{max} = 399 nm in 3 min
6	Present work	Co_3O_4 NPs prepared by HPCM method using *Azadirachta indica*	(a) Photocatalytic degradation of textile dye waste. (b) Reduction of 4-nitrophenol and 4-nitroaniline	(a) 73.8% degradation achieved in 150 min (b) reduction occurred at λ_{max} = 399 nm in 3 min

Table 3 Comparison of antibacterial activity of Co_3O_4-NPs with chloramphenicol standard

	Zone of inhibition (mm)	
Bacteria	Chloramphenicol	Co_3O_4
Staphylococcus aureus	10.6	16.3
Bacillus subtilis	20.8	22.2
Pseudomonas aeruginosa	20.5	34.5
Escherichia coli	20.1	16.4

controlled chemical reaction that converts the nitro group to the amine group in the presence of the Co_3O_4-NPs without any observable side reactions or by-products. Moreover, no reaction occurred in the absence of Co_3O_4-NPs. A similar trend was observed for the reduction of 4-nitroaniline; there was a significant decrease in absorption at 394 nm within 180 s, and Scheme 2 depicts the schematic of the catalytic hydrogenation of 4-nitrophenol and 4-nitroaniline. These reactions proceeded under mild conditions, (*i.e.*) at room temperature and in an aqueous medium, thereby implying probable use in the treatment of industrial toxic waste water. Nitro-organic effluents of $NaBH_4$ are also toxic, however this toxic effect is reduced because the reaction mechanism involves the production of sodium borohydroxide ($NaBH_2(OH)_2$). The catalytic activity of Co_3O_4-NPs towards the photocatalytic degradation of dyes and catalytic reduction of nitro-aromatics was compared with other reports, as is shown in Table 2.

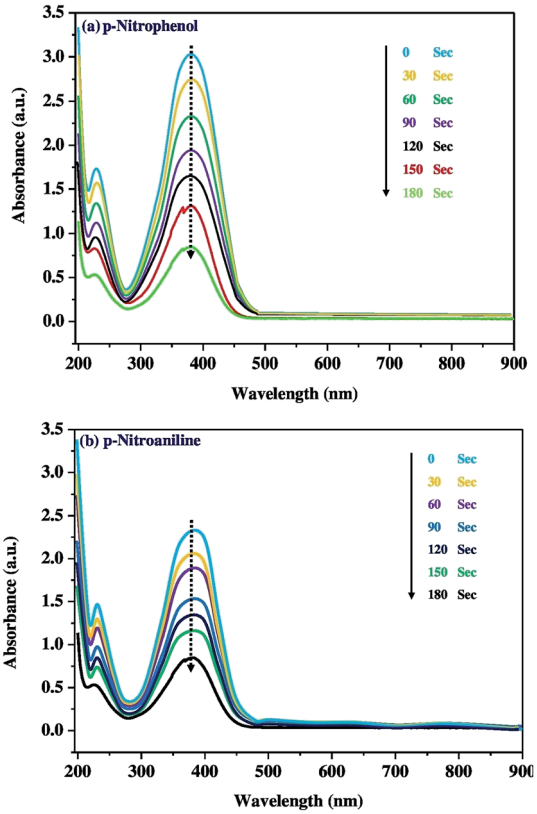

Fig. 5 Zone of inhibition produced by Co_3O_4-NPs against the bacterial strains (a) *Staphylococcus aureus*, (b) *Bacillus subtilis*, (c) *Pseudomonas aeruginosa*, and (d) *Escherichia coli*.

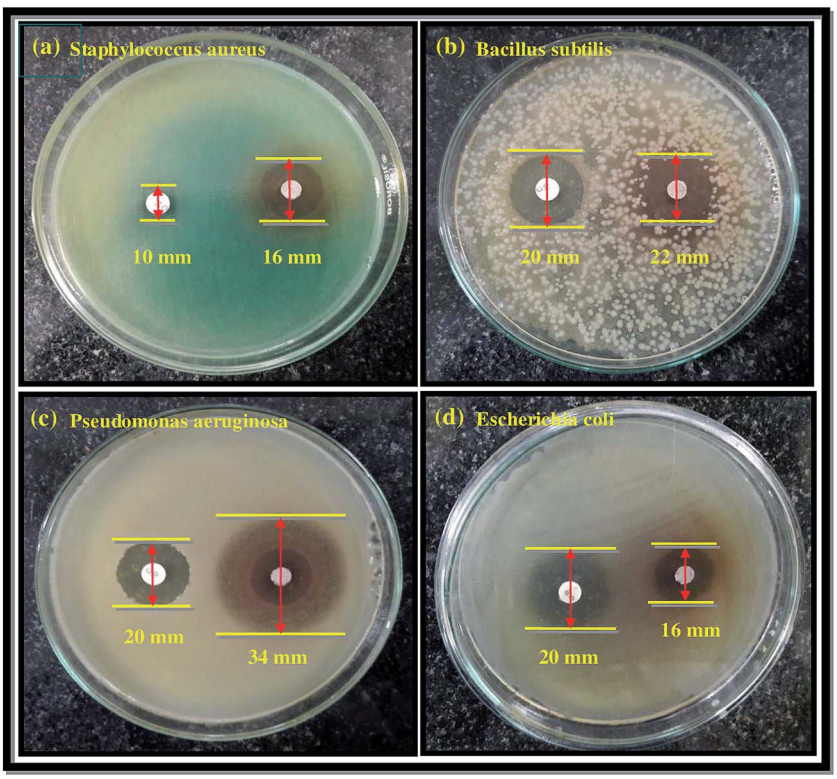

Fig. 4 Inhibitory effect of Co_3O_4-NPs in comparison with standard chloramphenicol against bacterial strains.

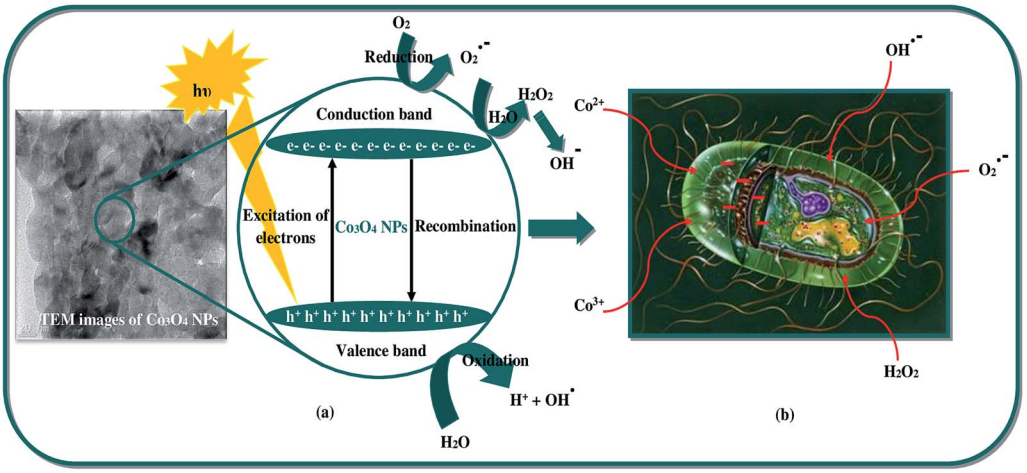

Scheme 3 Schematic of (a) •OH formation by light irradiation, (b) inhibitory activity of bacterial growth using Co_3O_4-NPs.

The as-synthesized Co_3O_4-NPs were evaluated for their antibacterial potential against both Gram positive and Gram negative bacterial strains. Gram positive (*Staphylococcus aureus* and *Bacillus subtilis*) and Gram negative bacterial strains (*Pseudomonas aeruginosa* and *Escherichia coli*) were selected for this assessment. Chloramphenicol (CP = 10 mcg) was utilized as a standard in order to contrast the consequences of bacterial inhibition using Co_3O_4-NPs. The zone of inhibition (mm) values against both the Gram positive and Gram negative bacterial strains for Co_3O_4-NPs and the standard CP are listed in Table 3, and the inhibitory effect of Co_3O_4-NPs in comparison with the standard CP are plotted in Fig. 4. The antibacterial activity experiments have established that the Co_3O_4-NPs displayed outstanding antagonistic effects on both Gram positive and Gram negative bacterial strains compared to the standard CP, and the respective diameter of the inhibition zones in the bacterial strains are due to the antibacterial potential of the Co_3O_4-NPs and CP (Fig. 5). The differences in the susceptibility of different bacterial strains is due to the differences in their oxidative stress tolerance.[49,50] The antibacterial potential mainly depends upon the particle size, specific surface area and morphology of the Co_3O_4-NPs; however, the clear mechanistic pathway for the inhibitory action of nanoparticles is still ambiguous. Few experimental studies have reported that this antibacterial potential is due to the result of an electrostatic interaction between the bacterial cell and the nanoparticles, which are capable of generating reactive oxygen species (ROS), a factor responsible for the bacterial cell destruction.[51] In this point of view, two probable mechanistic pathways can be recommended as shown in Scheme 3. In the first pathway, the different positive oxidation states of cobalt ions (Co^{2+} and Co^{3+}) in Co_3O_4-NPs can have a strong interaction with the negative part of the bacterial cell, thus leading to the destruction of bacterial cell.[52] The other possible pathway happens, due to the irradiation of light on the surface of Co_3O_4-NPs, which can lead to the formation of an excited electron in the conduction band and positive hole in the valence band, respectively. The excited electron in the conduction band react with the oxygen molecule to yield the superoxide radical anion ($O_2^{-\bullet}$), followed by the generation of hydrogen peroxide, a strong oxidizing agent. On the supplementary reaction of superoxide radical anion with water on the surface of Co_3O_4-NPs, the bacterial strain is ruined completely. Simultaneously, the positive hole in the valence band can react with water and produce hydroxyl radicals (•OH). Although hydroxyl radicals and superoxide radicals do not have any effect on penetration inside the cell membrane, they remain in contact with the outer layer of the bacterial cell and break down the proteins and lipids. Thus, the antibacterial potential of Co_3O_4-NPs at nano level concentrations finds greater effect for the destruction of microbial organisms.

Conclusion

In the present study, Co_3O_4-NPs were synthesized by a green and simple synthetic process using *A. indica* leaf extract by an efficient and simple HPCM. Co_3O_4-NPs were characterized by various techniques to depict their structural, morphological, optical and magnetic properties. The characterized properties include a good crystalline and hollow sphere like NPs with antiferromagnetic nature. Among the studies, the applications of the Co_3O_4-NPs in different fields like the PCD process, antibacterial analysis and catalytic reduction, were examined. Finally, excellent results were obtained in all the three applications, as reported herein. Hence, multifunctional Co_3O_4-NPs can be used for environmental remediation.

Acknowledgements

We thank Rev. Dr S. Lazar, S. J. Secretary, Loyola College for the infrastructure facilities given to carry out the present work successfully and authors (R. J and HAA) thank deanship of scientific research, King Saud University, funding through Vice deanship of scientific Research Chair.

References

1 J. Mittal, A. Batra, A. Singh and M. M. Sharma, *Adv. Nat. Sci.: Nanosci. Nanotechnol.*, 2014, **5**, 043002–043012.

2 S. Ahmed, M. Ahmad, B. L. Swami and S. Ikram, *J. Adv. Res.*, 2016, **7**, 17–28.
3 H. Padalia, P. Moteriya and S. Chanda, *Arabian J. Chem.*, 2015, **8**, 732–741.
4 B. Sadeghi and F. Gholamhoseinpoor, *Spectrochim. Acta, Part A*, 2015, **134**, 310–315.
5 S. Ashokkumar, S. Ravi and S. Velmurugan, *Spectrochim. Acta, Part A*, 2013, **115**, 388–392.
6 P. Logeswari, S. Silambarasan and J. Abraham, *Sci. Iran.*, 2013, **20**, 1049–1054.
7 P. R. R. Sre, M. Reka, R. Poovazhagi, M. A. Kumar and K. Murugesan, *Spectrochim. Acta, Part A*, 2015, **135**, 1137–1144.
8 A. Nabikhan, K. Kandasamy, A. Raj and N. M. Alikunhi, *Colloids Surf., B*, 2010, **79**, 488–493.
9 G. Brahmachari, *Chem. Bio. Chem.*, 2004, **5**, 408–421.
10 A. Akhila and K. Rani, *Fortschr. Chem. Org. Naturst.*, 1999, **78**, 47–149.
11 K. Biswas, I. Chattopadhyay, R. K. Banerjee and U. Bandyopadhyay, *Curr. Sci.*, 2002, **82**, 1336–1345.
12 R. Subapriya and S. Nagini, *Curr. Med. Chem.: Anti-Cancer Agents*, 2005, **5**, 149–156.
13 M. Manickam, V. Ponnuswamy, C. Sankar and R. Suresh, *Optik*, 2016, **127**, 5278–5284.
14 Y. Ikedo, J. Sugiyama, H. Nozaki and H. Itahara, *Phys. Rev. B: Condens. Matter Mater. Phys.*, 2007, **75**, 054424–054428.
15 N. Sattarahmady and H. Heli, *J. Exp. Nanosci.*, 2012, **7**, 529–546.
16 X. Wang, X. L. Wu, Y. G. Guo, Y. Zhong, X. Cao, Y. Ma and J. Yao, *Adv. Funct. Mater.*, 2010, **20**, 1680–1686.
17 C. Yuan, L. Hou, L. Shen, D. Li, F. Zhang, C. Fan, J. Li and X. Zhang, *Electrochim. Acta*, 2010, **56**, 115–121.
18 J. Jiang and L. Li, *Mater. Lett.*, 2007, **61**, 4894–4896.
19 Z. Dong, Y. Fu, Q. Han, Y. Xu and H. Zhang, *J. Phys. Chem. C*, 2007, **111**, 18475–18478.
20 H. Singh, A. K. Sinha, M. N. Singh, P. Tiwari, D. M. Phase and S. K. Deb, *J. Phys. Chem. Solids*, 2014, **75**, 397–402.
21 H. Linhua, P. Qing and L. Yadong, *J. Am. Chem. Soc.*, 2008, **130**, 16136–16137.
22 K. Zheng, M. I. Setyawati, T. P. Lim, D. T. Leong and J. Xie, *ACS Nano*, 2016, **10**, 7934–7942.
23 K. Zheng, M. I. Setyawati, D. T. Leong and J. Xie, *ACS Nano*, 2017, **11**, 6904–6910.
24 Y. Liu, Q. Yao, X. Wu, T. Chen, Y. Ma, C. N. Onga and J. Xie, *Nanoscale*, 2016, **8**, 10145–10151.
25 S. Kuboon and Y. H. Hu, *Ind. Eng. Chem. Res.*, 2011, **50**, 2015–2020.
26 L. M. Alrehaily, J. M. Joseph and J. C. Wren, *Phys. Chem. Chem. Phys.*, 2015, **17**, 24138–24150.
27 R. F. K. Gunnewiek, C. F. Mendes and R. H. G. A. Kiminami, *Adv. Powder Technol.*, 2016, **27**, 1056–1061.
28 C. J. Denis, C. J. Tighe, R. I. Gruar, N. M. Makwana and J. A. Darr, *Cryst. Growth Des.*, 2015, **15**, 4256–4265.
29 A. Diallo, A. C. Beye, T. B. Doyle, E. Park and M. Maaza, *Green Chem. Lett. Rev.*, 2015, **8**, 30–36.
30 V. D. Mote, Y. Purushotham and B. N. Dole, *Ceramica*, 2013, **59**, 614–619.
31 X. Xia, J. Tu, X. Wang, C. Gu and X. Zhao, *Chem. Commun.*, 2011, **47**, 5786–5788.
32 Q. Liu, J. Tian, W. Cui, P. Jiang, N. Cheng, A. M. Asiri and X. Sun, *Angew. Chem., Int. Ed.*, 2014, **53**, 6710–6714.
33 S. Farhadi, J. Safabakhsh and P. Zaringhadam, *J. Nanostruct. Chem.*, 2013, **3**, 69–77.
34 R. A. Tuwirqi, A. A. Al-Ghamdi, N. A. Aal, A. Umar and W. E. Mahmoud, *Superlattices Microstruct.*, 2011, **49**, 416–421.
35 Y. G. Zhang, Y. C. Chen, T. Wang, J. H. Zhou and Y. G. Zhao, *Microporous Mesoporous Mater.*, 2008, **114**, 257–261.
36 A. Azam, *J. Alloys Compd.*, 2012, **540**, 145–153.
37 M. Y., *Mater. Lett.*, 2013, **94**, 112–115.
38 C. Cao, C. Hu, W. Shen, S. Wang, H. Liu and J. Wang, *Sci. Adv. Mater.*, 2013, **5**, 1256–1263.
39 Y. Koseoglu, F. Kurtulus, H. Kockar, H. Guler, O. Karaagac, S. Kazan and B. Aktas, *J. Supercond. Novel Magn.*, 2012, **25**, 2783–2787.
40 S. K. Jesudoss, J. J. Vijaya, L. J. Kennedy, P. I. Rajan, H. A. Al-Lohedan, R. J. Ramalingam, K. Kaviyarasu and M. Bououdina, *J. Photochem. Photobiol., B*, 2016, **165**, 121–132.
41 P. Suresh, J. J. Vijaya, T. Balasubramaniam and L. J. Kennedy, *Desalin. Water Treat.*, 2014, **57**, 1–16.
42 H. Pablo, P. L. Moise, M. L. Luis, D. Joachim, L. Yan and B. Matthias, *Chem. Soc. Rev.*, 2012, **31**, 5577–5587.
43 H. Linhua, P. Qing and L. Yadong, *J. Am. Chem. Soc.*, 2008, **130**, 16136–16137.
44 C. R. Dhas, R. Venkatesh, K. Jothivenkatachalam, A. Nithya, B. S. Benjamin, A. M. EzhilRaj, K. Jeyadheepan and C. Sanjeeviraja, *Ceram. Int.*, 2015, **41**, 9301–9313.
45 S. Farhadi, M. Javanmard and G. Nadri, *Acta Chim. Slov.*, 2016, **63**, 335–343.
46 I. Bibi, N. Nazar, M. Iqbal, S. Kamal, H. Nawaz, S. Nouren, Y. Safa, K. Jilani, M. Sultan, S. Ata, F. Rehman and M. Abbas, *Adv. Powder Technol.*, 2017, **28**, 2035–2043.
47 A. Sharma, R. K. Dutta, A. Roychowdhury, D. Das, A. Goyal and A. Kapoor, *Appl. Catal., A*, 2017, **543**, 257–265.
48 J. Krajczewski, K. Kołataj and A. Kudelski, *Appl. Surf. Sci.*, 2016, **388**, 624–630.
49 Y. Liu, Y. Zheng, B. Du, R. R. Nasaruddin, T. Chen and J. Xie, *Ind. Eng. Chem. Res.*, 2017, **56**, 2999–3007.
50 Y. Liu, L. Yu, C. N. Ong and J. Xie, *Nano Res.*, 2016, **9**, 1983–1993.
51 P. K. Stoimenov, R. L. Klinger, G. L. Marchin and K. J. Klabunde, *Langmuir*, 2002, **18**, 6679–6686.
52 Y. Liu, J. Xie, C. N. Ong, C. D. Vecitis and Z. Zhou, *Environ. Sci.: Water Res. Technol.*, 2015, **1**, 769–778.

